An Article for Publication in *Nature Materials*

One-Dimensional Imidazole Aggregate in Aluminum Porous Coordination Polymers with High Proton Conductivity

Sareeya Bureekaew[1,5], Satoshi Horike[1,5], Masakazu Higuchi[2], Motohiro Mizuno[3], Takashi Kawamura[1], Daisuke Tanaka[1], Nobuhiro Yanai[1], Susumu Kitagawa[1,4,5]

(1) Department of Synthetic Chemistry and Biological Chemistry, Graduate School of Engineering, Kyoto University, Katsura, Nishikyo-ku, Kyoto 615-8510, Japan,

(2) RIKEN, SPring-8 center, 1-1-1, Kouto, Sayo-cho, Sayo-gun, Hyogo 679-5148, Japan

(3) Department of Chemistry, Graduate School of Natural Science and Technology, Kanazawa University, Kanazawa 920-1192, Japan

(4) Institute for Integrated Cell-Material Sciences (iCeMS) Kyoto University, Yoshida, Sakyo-ku, Kyoto 606-850, Japan,

(5) Kitagawa Integrated Pore Project, Exploratory Research for Advanced Technology (ERATO), Japan Science and Technology Agency (JST), Kyoto Research Park, 134 Chudoji Minami-machi, Shimogyo-ku, Kyoto 600-8813, Japan

CORRESPONDING AUTHOR FOOTNOTE

Dr. Susumu Kitagawa
Department of Synthetic Chemistry and Biological Chemistry,
Graduate School of Engineering, Kyoto University
Katsura, Nishikyo-ku, Kyoto 615-8510, Japan
TEL: +81-75-383-2833
FAX: +81-75-383-2732
e-mail: kitagawa@sbchem.kyoto-u.ac.jp

ABSTRACT: *The development of anhydrous proton-conductive materials operating at temperatures above 80 ℃ is a challenge that needs to be met for practical applications. Herein, we propose the new idea of encapsulation of a proton-carrier molecule—imidazole in this work—in aluminum porous coordination polymers for the creation of a hybridized proton conductor under anhydrous conditions. Tuning of the host–guest interaction can generate a good proton-conducting path at temperatures above 100 ℃. The dynamics of the adsorbed imidazole strongly affect the conductivity determined by ^{2}H solid-state NMR. Isotope measurements of conductivity using imidazole-d_4 showed that the proton-hopping mechanism was dominant for the conducting path. This work suggests that the combination of guest molecule and a variety of microporous frameworks would afford highly mobile proton carriers in solids and gives an idea for designing a new type of proton conductor, particularly for high temperature and anhydrous conditions.*

KEYWORDS: porous coordination polymer, metal–organic framework, proton conductivity, solid–state NMR

Anhydrous proton–conducting solids that are able to operate at high temperature (~120 °C) are required in fuel cell technology.[1,2] Heterocyclic organic molecules such as imidazole or benzyl imidazole have attracted considerable attention for this purpose because they are nonvolatile molecules with high boiling points, and they can exist in two tautomeric forms with respect to a proton that moves between the two nitrogen atoms, which supports a proton transport pathway.[3,4] The protonic defect may cause local disorder by forming protonated and unprotonated imidazoles. In such materials the proton transport may occur through structure diffusion which involves proton transfer between the imidazole and the imidazolium ion through the hydrogen–bonded chain, including the molecular reorientation process for subsequent intermolecular proton transfer.[1] Theoretically, the magnitude of the ionic conductivity is given as

$$\sigma(T) = \sum n_i q_i \mu_i \quad (1)$$

where n_i is the number of carriers, and q_i and μ_i are the charge and mobility of the carriers, respectively.[5] Both a large amount and a high mobility of ion carriers are required to provide good proton conductivity. Hence it is important to find suitable materials that meet these requirements. For instance, solid imidazole has a low conductivity (~10^{-8} S cm^{-1}) at ambient temperature[6] although the imidazole density (n_i) is adequately high. This is because the dense packing of imidazole, with strong hydrogen bonding in the solid state, decreases the mobility of each molecule (μ_i).

The main goal of proton conductor modification should therefore be an improvement of the mobility of proton carriers. It is known that local and translational motion of proton carriers strongly affect the proton transfer rate.[1] In order to control the mobility of proton carriers, additional support matrices such as flexible organic polymers or high-porosity solids that afford movable space for a carrier are considered promising.

Porous coordination polymers (PCPs) or metal organic frameworks constructed from transition metal ions and organic ligands have received much attention over the past few years because of their promising applications, such as in gas storage,[7-11] separation,[12-17] catalysis,[18-26] and conductivity.[27-29] Recent developments in approaches to combine PCP frameworks and functional guests such as polymers,[30,31] metals,[22,32-34] or small organic molecules[35-37] on a molecular scale have prompted us to create hybrid materials with novel performance based on the feature that crystalline nanochannels can afford a unique assembly field for functional guests with specific host–guest interactions. The guests in the nanospace of PCPs exhibit unusual behavior compared to in the bulk phase because each manner of assembly is heavily dependent on the nature of the PCP channels, such as their size, shape and chemical environment. Hence, we propose the use of PCPs for incorporation with proton carrier molecules because they can contribute to provide desirable working space for carrier molecules, with high mobility, and show an appropriate packing structure, for improved proton conductivities at high temperatures and under anhydrous conditions (Figure 1).

In this study we focused on two types of PCPs with 1D channels and high thermal stability (~400 °C), and imidazole as the guest proton carrier molecule. Taking the size and shape of imidazole (4.3 × 3.7 Å^2) into consideration, we chose to use the aluminum compounds [Al(μ_2-OH)(1,4-ndc)]$_n$ (**1**; 1,4-ndc = 1,4-naphthalenedicarboxylate)[38] and [Al(μ_2-OH)(1,4-bdc)]$_n$ (**2**; 1,4-bdc = 1,4-benzenedicarboxylate),[9,39] both of which have pore dimensions of ca. 8 Å, but different pore shapes and surface potential, and installed imidazole in each host material. We found that the nanochannels potentiated the different packing of imidazole, compared with the bulk solid imidazole. Conductivity measurements for each of the PCP–imidazole composites at various temperatures and under anhydrous condition presented different profiles because of the different characteristics of the channels of the respective PCPs, resulting in different host–guest interactions, and **1**⊃Im had a conductivity of 2.2 × 10^{-5} S cm^{-1} at 120 °C. We investigated the behavior of absorbed imidazole in the micropores by means of the solid-state NMR technique, and succeeded in determining a good correlation between the features of the host channels, guest mobility and proton conductivity.

Structural information of 1 and 2

The structures of **1** and **2** comprise an infinite number of chains of corner–sharing $AlO_4(\mu_2\text{-}OH)_2$ interconnected by the dicarboxylate ligand, resulting in a 3D framework containing 1D channels. The guest–free structures of **1** and **2** are shown in Figure 2. Crystallographic structures show that the pore surfaces of **1** and **2** are composed of hydrophobic (aromatic naphthalene and benzene ring) and hydrophilic ($AlO_4(\mu_2\text{-}OH)_2$) parts. The principal difference between the two aluminum frameworks arises from the difference in ligands 1,4-ndc and 1,4-bdc. Because of asymmetric bridging ligand, **1** consists of two kinds of rectangular channels with dimensions of 7.7 × 7.7 Å^2 and 3.0 × 3.0 Å^2 running along the *c* axis (Figure 2a). This compound shows the property of a rigid framework. Figure 2b shows that steric hindrance arising from the bulky naphthalene ring of the 1,4-ndc ligand of **1** induces restriction of interaction between the polar guest molecule and μ_2-OH and/or carboxylate group of the framework. Because of the absence of an accessible hydrophilic pore surface the hydrophobic character from the aromatic part of the naphthalene ring of the ligand is dominant. In other words, **1** provides two types of microchannels with hydrophobic pore surfaces.

In the case of **2** the framework exhibits only 1D diamond–shaped channels composed of the smaller benzene moieties of 1,4-bdc, with dimensions 8.5 × 8.5 Å^2, running along the *a* axis. Eventually, the polar sites on the surface are exposed to guest molecules, which enhances guest–induced structural transformation of **2,** with the aid of the interaction between the imidazoles and μ_2-OH and/or a carboxylate groups.[40] Thus, it is intriguing that a simple modification on the organic moiety produces channels with different nature, hydrophobic and hydrophilic for **1** and **2,** respectively. [39]

Properties of the inclusion compounds

The thermogravimetric (TG) profiles of **1**⊃Im and **2**⊃Im are shown in Figure 3. Note that**1**⊃Im and **2**⊃Im indicate the imidazole hybrid compound of **1** and **2**, respectively. The existence of imidazole in **1** and **2,** without any reactions/conversion, was confirmed by thermogravimetry/mass spectrometry (TG–MS). The TG profile of **1**⊃Im shows 14% weight imidazole loading or 0.6 imidazole/1 Al ion. The release of accommodated imidazole commences at 160 °C and completes at 225 °C. In the case of **2,** the loaded imidazole amounts to 30% weight or 1.3 imidazole/1 Al ion, which is twice as much as in **1**. The TG curve shows that the loss of imidazole molecules in **2**⊃Im occurs in two steps: in the first step, the release of imidazole commences at 130 °C and is completed by approximately 160 °C and in the second step it commences at 160 °C and is completed by 240 °C. The percentage imidazole loss is half the amount of the imidazole, followed by the residual in the second step.

The one single step mass loss in **1**⊃Im is indicative of uniformly accommodated imidazole molecules. On the other hand, based on the TG curve of **2**⊃Im, there are two types of imidazole molecules installed in the channel. According to the amphiphilic nature of the surface of the channel, the imidazoles with strong interaction with the hydrophilic sites of a μ_2-OH or a carboxylate group are released at higher temperature (160 – 240 °C), correlated to the weight loss in second step, whereas the imidazoles which have less interaction with pore surface are removed in the first step (below 160 °C).

The crystal structures of **1** and **2** (Figure 2) reveal the following. Compound **1** consists of two types of 1D channels, namely small channels with dimensions 3.0 × 3.0 $Å^2$ in which imidazole is unable to be installed: only large channels with dimensions of 7.7 × 7.7 $Å^2$ can install the guest. Compared with **2**⊃Im, half the amount of accommodating imidazole per one Al is reasonable from crystal structures.

Considering that the dispersion of imidazole is uniform in the crystalline channel we could calculate the density of imidazole in the larger channels of **1** (443 $Å^3$) and channels of **2** (750 $Å^3$). This was calculated from the void space of the guest–free state by using the PLATON software package.[41] The values were about 0.15 and 0.19 g cm^{-3}, respectively. However, as the structure of **2** changes after accommodation of imidazole and it is difficult to determine the density of imidazole in **2**⊃Im. The density of imidazoles in **1**⊃Im and **2**⊃Im are much smaller than that of solid bulk imidazole, which is 1.23 g cm^{-3} at ambient temperature.[42] This evidence indicates that the behaviors of imidazoles loaded to the framework considerably differ from bulk imidazole resulting from the space effect.

The X–ray powder diffraction (XRPD) patterns shown in Figure 4 show that the diffraction pattern of **1**⊃Im is the same as that of apohost **1**, corresponding to the robustness of **1**. Conversely, the peak positions and pattern of **2**⊃Im are different from those of apohost **2** and the shrinkage after installation of imidazole is observed. This is because of strong interaction between the polar imidazole and hydrophilic pore surface of flexible **2**.

Conductivity of 1⊃Im and 2⊃Im

We aimed to achieve proton conductivity at temperatures around 100 °C, and hence to design composites that are stable at the target temperatures. We already confirmed that the prepared composites **1**⊃Im and **2**⊃Im are stable up to 130 °C without any loss from TG. Conductivities of **1**⊃Im and **2**⊃Im were measured by AC impedance spectroscopy, which is a versatile electrochemical tool to characterize intrinsic electrical properties of materials. Figure 5b and 5c shows Nyquist plots (Z' versus Z'') of the complex impedance measured on **1**⊃Im and **2**⊃Im under a nitrogen atmosphere at 120 °C. The impedance plots of the two complexes are typical of materials with predominant ionic conductivity.

They show one semicircle with a characteristic spur at low frequencies, which indicates blocking of H^+ ions at the gold electrodes. The magnitude of Z' decreased with an increase in temperature. The conductivity of the samples was calculated from the impedance value using the following equation

$$\sigma = \frac{L}{Z \cdot A} \qquad (2)$$

where σ is the conductivity (S cm^{-1}), L is the measured sample thickness (cm), A is the electrode area (cm^2) and Z is the impedance (Ω).

The temperature dependence of proton conductivities of **1**, **1**⊃Im and **2**⊃Im, measured under anhydrous conditions at temperatures ranging from 25 to 120 °C, are shown in Figure 5a. Guest−free **1** exhibits a conductivity lower than 10^{-13} S cm^{-1}, confirmed by DC measurement, which is indicative of negligible proton conductivity for this apohost framework. After installation of imidazole the proton conductivity of **1**⊃Im is 5.5×10^{-8} S cm^{-1} at room temperature. Although the mole fraction of imidazole in **1**⊃Im is much smaller than that of bulk imidazole, the proton conductivity of **1**⊃Im is of the same order as that of solid bulk imidazole. This is possibly because of the effect of the nanospace on the dynamic motion of imidazole. The proton conductivity of **1**⊃Im improves significantly as the temperature increases: at 120 °C the proton conductivity reaches 2.2×10^{-5} S cm^{-1}. Note that bulk imidazole at this temperature is no longer in the solid phase. This increase in the temperature dependent conductivity of **1**⊃Im, compared with the conductivity profile of apohost **1**, indicates that a significant improvement in the conductivity arises directly from the accommodated imidazole. Furthermore, the conductivity of **1**⊃Im continuously increases with an increase in temperature with the activation energy of 0.6 eV. This result indicates that phase transition does not take place. The mobile imidazole induces high temperature (> 100 °C) proton conductivity in **1**⊃Im. We can improve the mobility of imidazole by taking advantage of the isolating effect of PCPs. As the evidence from isotope effect (Figure S1), the proton conductivity of our systems is mainly contributed by proton hopping mechanism.

In order to improve proton conductivity we increased the amount of loaded imidazole (the number of charge carriers, n_i) by using **2**, which has twice the amount of accessible space for imidazole as the supporting framework. However, the proton conductivity of **2**⊃Im at ambient temperature is about 10^{-10} S cm^{-1}, which is lower than that of **1**⊃Im. As in the case of **1**⊃Im, the conductivity of **2**⊃Im increases as the temperature increases with the activation energy of 0.9 eV, and it reaches 1.0×10^{-7} S cm^{-1} at 120 °C. The proton conductivity of **2**⊃Im is about two orders of magnitude lower than that of **1**⊃Im, although the amount of loaded imidazole is higher than that of **1**⊃Im. This is also possibly because of the difference in dynamic motion of the guest, which is based on the interaction between guest and host. Microchannels in compound **1** have nonpolar potential surface and polar imidazole does not interact strongly with the host framework; therefore, it can move freely in this channel. Nonetheless, in the case of polar surface microchannels in **2**, the half amount of imidazole interact strongly with the hydrophilic sites of host framework. The strong host–guest interactions give rise to the shrinkage of the framework, eventually of a unit cell, resulting in the different environment of imidazole accommodated in **2**, compared to in **1**. Therefore, because of strong host–guest interaction and dense packing, the imidazoles with strong interaction with the μ_2-OH and/or carboxylate group of **2** are not allowed to move or rotate freely in the framework. Consequently, the conductivity in **1**⊃Im is larger than in **2**⊃Im.

Direct observation of dynamics of imidazoles in 1⊃Im and in 2⊃Im

Solid-state ^{2}H NMR spectroscopy is suitable for examining the dynamics of target molecules selectively.[43-45] We therefore used this analytical technique to determine the mobility and its correlation with the conductivity of adsorbed imidazole in **1** and **2**. The ^{2}H NMR powder line shapes are sensitive to local molecular motion and are characterized in terms of both the time scale and the mode of the motion, such as rotation or wobbling behavior.[46,47] We introduced imidazole-d_4 for each host instead of nondeuterated imidazole and checked that the adsorbed amount for each guest was identical to that in the normal hosts. The ^{2}H NMR spectra of **1**⊃Im and **2**⊃Im recorded at different temperatures are shown in Figure 6. In the case of **2**⊃Im (Figure 6b), at the lowest measured temperature of 20 °C, we observed a clear Pake-type doublet pattern with a splitting width of 120 kHz, indicating that the adsorbed imidazole-d_4 behaves totally anisotropically. As the temperature increases, a narrow Lorentzian-type peak appears in the middle of the anisotropic powder pattern, corresponding to the emergence of isotropic imidazole by thermal activation. There are two possible explanations for the spectrum: the first is that free motional imidazole with low frequency shows a narrow peak and the second is the simultaneous coexistence of frequencies of slow and fast imidazole. Nonetheless, the spectrum at 40 °C indicates the existence of activated guests in pores, and the relative intensity of the activated species increases as the temperature increases to 80 °C.

In the case of **1**⊃Im, spectra also show doublet powder patterns at low temperatures (–20 and –60 °C) with the same splitting width as in **2**⊃Im at temperatures lower than 30 °C. However, a narrow Lorentzian-type peak starts to appear at 20 °C. This clearly indicates that at ambient temperature the imidazole in **1** can show isotropic motion with a larger frequency than **2**. The fraction of isotropic imidazole becomes dominant at 40 °C, and at 80 °C we can no longer observe any Pake-doublet pattern at all. This suggests that all adsorbed imidazole within the pores of **1** has a fast isotropic motion. Using the NMR line shapes obtained, we evaluated the motion of the imidazole using a simulation procedure. We used a free rotation model of imidazole molecules with tetrahedral orientations as the main motion because this is associated with the Grotthus mechanism. We succeeded in obtaining theoretical patterns for both samples, at each temperature, based on the tetrahedral free rotational model as shown in Figure 6, and clearly observed that the rotation frequency of **1** is greater than that of **2**. For example, the frequency of **1** at 60 °C is 45 kHz whereas that of **2** shows 10 kHz, while the frequency of **1** at 20 ºC (20 kHz) is still larger than that of **2** at 90 ºC (18 kHz) (see Figure S2). Consequently, we are able to conclude that the degree of motional behavior of the accommodated imidazole of **1** is greater than in the case of **2**, which strongly supports the difference in conductivity.

We have presented a new approach to create proton transportation space based on the use of proton carrier organic molecules to enhance the proton conductivity of solid materials under anhydrous conditions at high temperature. The different values of conductivity of imidazole in compounds **1** and **2** are consistent with the dynamic properties of imidazole adsorbed in the pores. The hydrophilic microporous surface of **2** results in strong interaction with even the half amount the adsorbed imidazoles and significantly decelerates their mobility, resulting in a poor proton transfer rate. On the other hand, because of the hydrophobic and flat pore surface of **1**, adsorbed imidazole can move more freely than in **2** and than bulk phase, and we eventually observe higher proton conductivity, which is comparable to that of a conventional organic polymer conductor such as poly(4-vinylimidazole).[48] PCP can provide an appropriate pore environment and size for target proton carrier by the fine–tuning of their components. In the other word, the optimum mobility and density of proton carriers can be reached by taking advantage of the designability of PCPs. The strategy would be considered significant to prepare hybrid materials high proton–conductive.

Experimental section

Materials

Aluminium(III) nitrate nanohydrate $Al(NO_3)_3{\cdot}9H_2O$ (WAKO, 99.9%); terephthalic acid $HO_2C–(C_6H_4)–CO_2H$ (WAKO, 95%); 1,4-naphthalene dicarboxylic acid $HO_2C–(C_{10}H_8)–CO_2H$ (WAKO, 95%); imidazole (WAKO, 99%) and imidazole (D–4, CIL, 98%) were used as received. Distilled water was used.

Synthesis of {Al(μ_2-OH)(1,4-ndc)}$_n$ (1)

A mixture of $Al(NO_3)_3{\cdot}9H_2O$ (0.375 g, 1.0 mmol); 1,4-naphthalene dicarboxylic acid (0.108 g, 0.5 mmol) and deionized water (10 mL) was placed in a 23 mL Teflon autoclave and heated at 180 °C for one day. The initial pH of the reaction mixture was 2.5 and the final pH was 2.0. After filtering and washing the crude product with distilled water, a pure, light-yellow powder of **1**$\cdot 2H_2O$ was obtained (yield 80%). The sample was evacuated at 150 °C for 12 hours to afford the guest-free compound **1**.

Synthesis of {Al(μ_2-OH)(1,4-bdc)}$_n$ (2)

The synthesis of **2** was carried out under hydrothermal conditions using $Al(NO_3)_3{\cdot}9H_2O$ (1.30 g, 3.5 mmol); 1,4-benzenedicarboxylic acid (0.288 g, 2.5 mmol) and distilled water (10 mL). The reaction was performed in a 23 mL Teflon autoclave. The reaction mixture was heated at 220 °C for three days. After filtering and washing with distilled water, a white powder was obtained. It was identified by powder X-ray diffraction analysis. The excess terephthalic acid in the pores was removed by high-temperature treatment at 330 °C for three days. X-ray powder diffraction (XRPD) analysis revealed that the material was the guest-free compound **2**.

Preparation of imidazole-loaded frameworks

Products **1** and **2** were again degassed by heating to 120 °C under reduced pressure for 12 h to remove guest molecules. Imidazole was vaporized into guest-free **1** and **2** at 120 °C, overnight, to yield **1**⊃Imi and **2**⊃Imi. XRPD patterns of both these compounds confirmed that the frameworks were maintained. The amount of loaded imidazole was determined by TG analysis.

Proton conductivity measurement of 1⊃Im and 2⊃Im

Samples for conductivity measurements were prepared by sandwiching the respective powders **1**⊃Im and **2**⊃Im between two gold-coating electrodes (diameter 3 mm) and then tightly connecting the two electrodes, by means of springs, to ensure good contact between the sample and each electrode. Temperature-dependent conductivities of **1**⊃Im and **2**⊃Im were determined using alternative current (AC) impedance spectroscopy (Solartron SI 1260 Impedance/Gain-Phase analyzer), using a homemade cell over the frequency range 1 Hz – 10 MHz and with an input voltage amplitude of 100 mV. The measurement cell was filled with nitrogen at atmospheric pressure prior to recording the measurements. ZView software was utilized to extrapolate impedance data results via equivalent circuit simulation to complete the Nyquist plot and obtain the resistance values.

^{2}H solid-state NMR

Solid-state ^{2}H NMR spectra were recorded using a Varian Chemagnetics CMX-300 spectrometer, at 45.826 MHz, and a quadrupole echo pulse sequence. Simulated spectra were produced with FORTRAN programs written by us.

FIGURE CAPTIONS

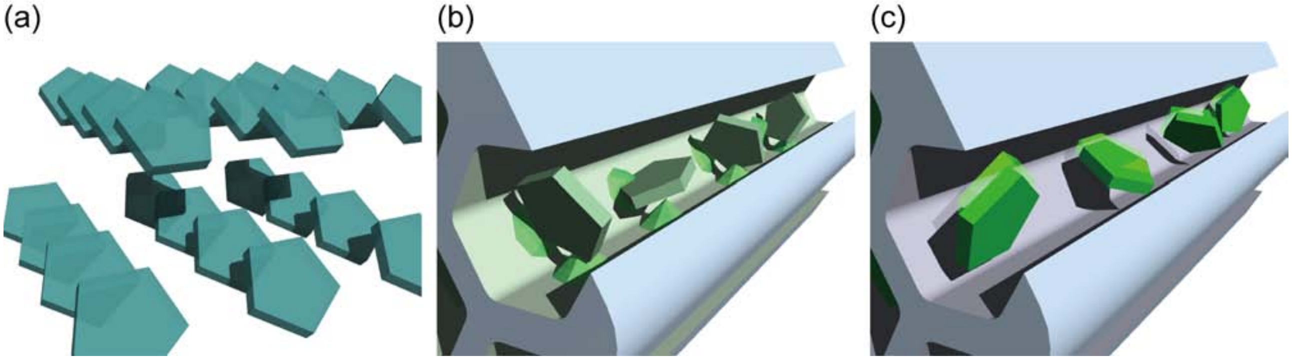

Figure 1. Imidazole molecules are densely packed with low mobility that adversely affects proton transport process. This occurs in the bulk solid (a). Imidazole accommodated in nanochannel containing the active site with a high affinity to imidazole. The strong host–guest interaction retards the mobility of imidazole to afford the low proton conductivity (b). Imidazoles are accommodated in nanochannel without strong host–guest interaction, and therefore, the molecules obtain the high mobility to show high proton conductivity (c).

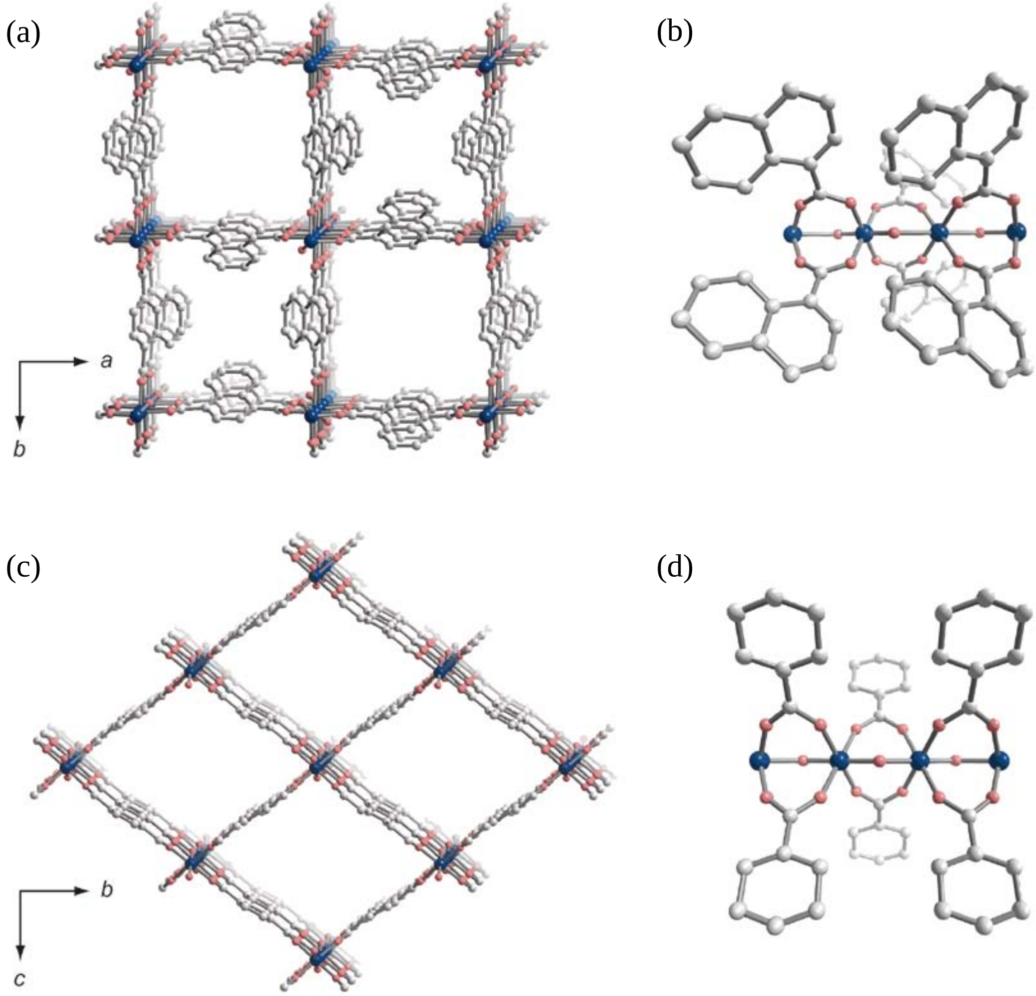

Figure 2. 3D structures of **1** (a) and **2** (c). Al, C, and O are represented in blue, gray, and red, respectively. H atoms are omitted for clarification. (b) and (d) show comparison of ligand size effect on μ_2-OH group of **1** and **2** respectively.

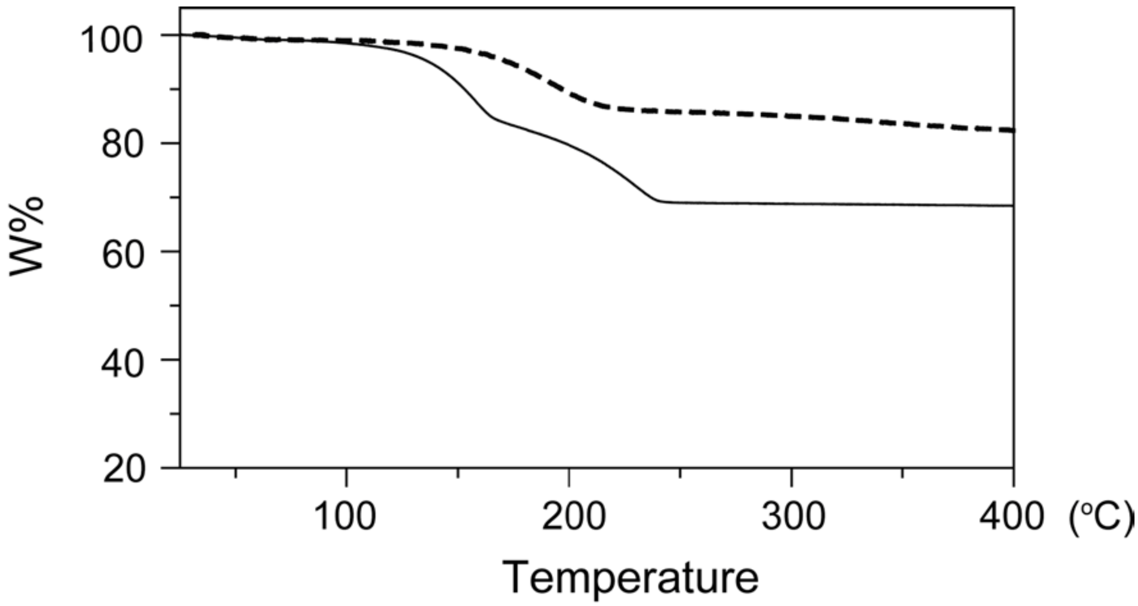

Figure 3. TGA curves for **1**⊃Im (dash line) and **2**⊃Im (solid line) over the temperature range from 25 – 400 °C at heating rate 10 °C min^{-1} under N_2 atmosphere. The guest release of **1**⊃Im occurs in one single step that clues the homogeneous installation of imidazole in **1**, whereas of **2**⊃Im occurs in two steps, indicating two types of imidazole (strongly and weakly interacts with **2**).

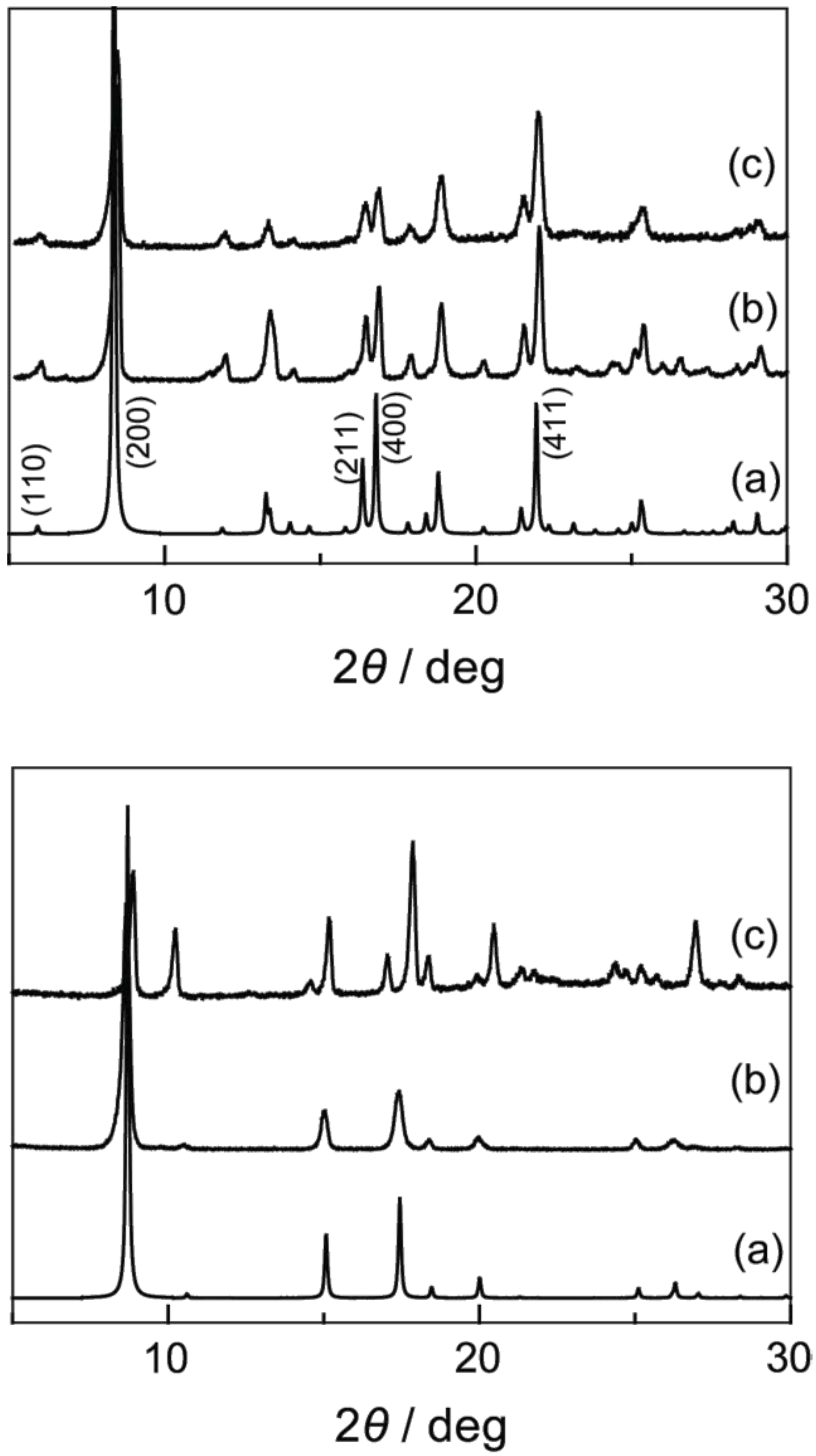

Figure 4. Above: XRPD patterns of simulated **1**·$2H_2O$ (a), **1** (b), and **1**⊃Im (c). The patterns before and after accommodation of imidazole are identical. Below: XRPD patterns of simulated **2** (a), **2** (b), and **2**⊃Im (c). A change in XRPD patterns after accommodation of imidazole is observed.[39]

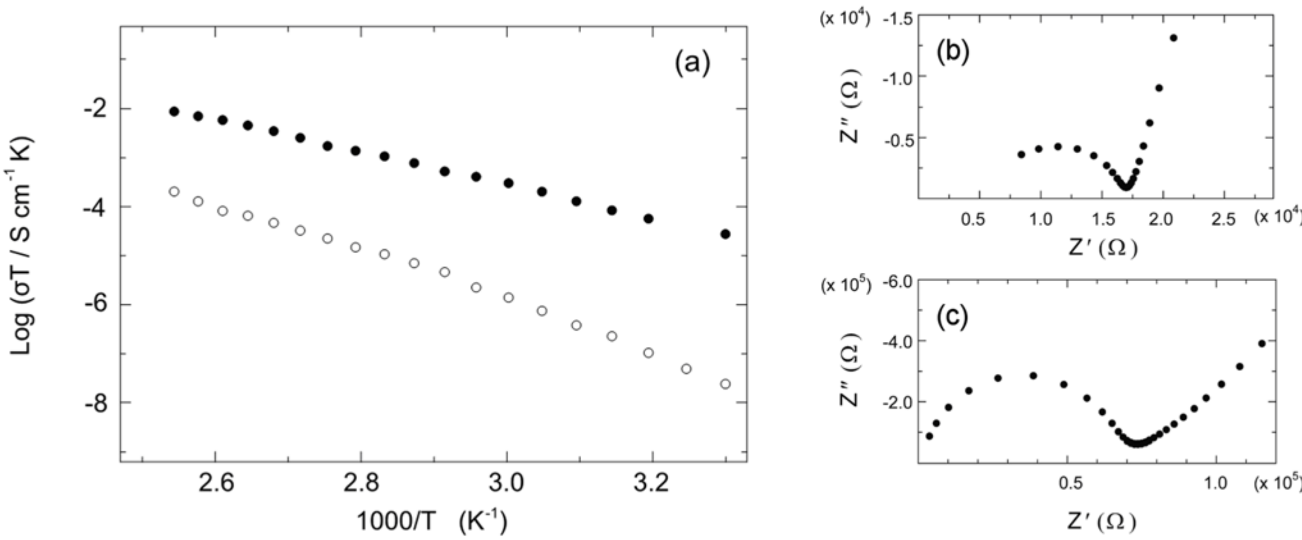

Figure 5. (a) Proton conductivity of **1**⊃Im (filled dots) and **2**⊃Im (empty dots) under anhydrous condition performed by A.C. impedance analyzer. Nyquist diagrams of **1**⊃Im (b) and **2**⊃Im (c) at

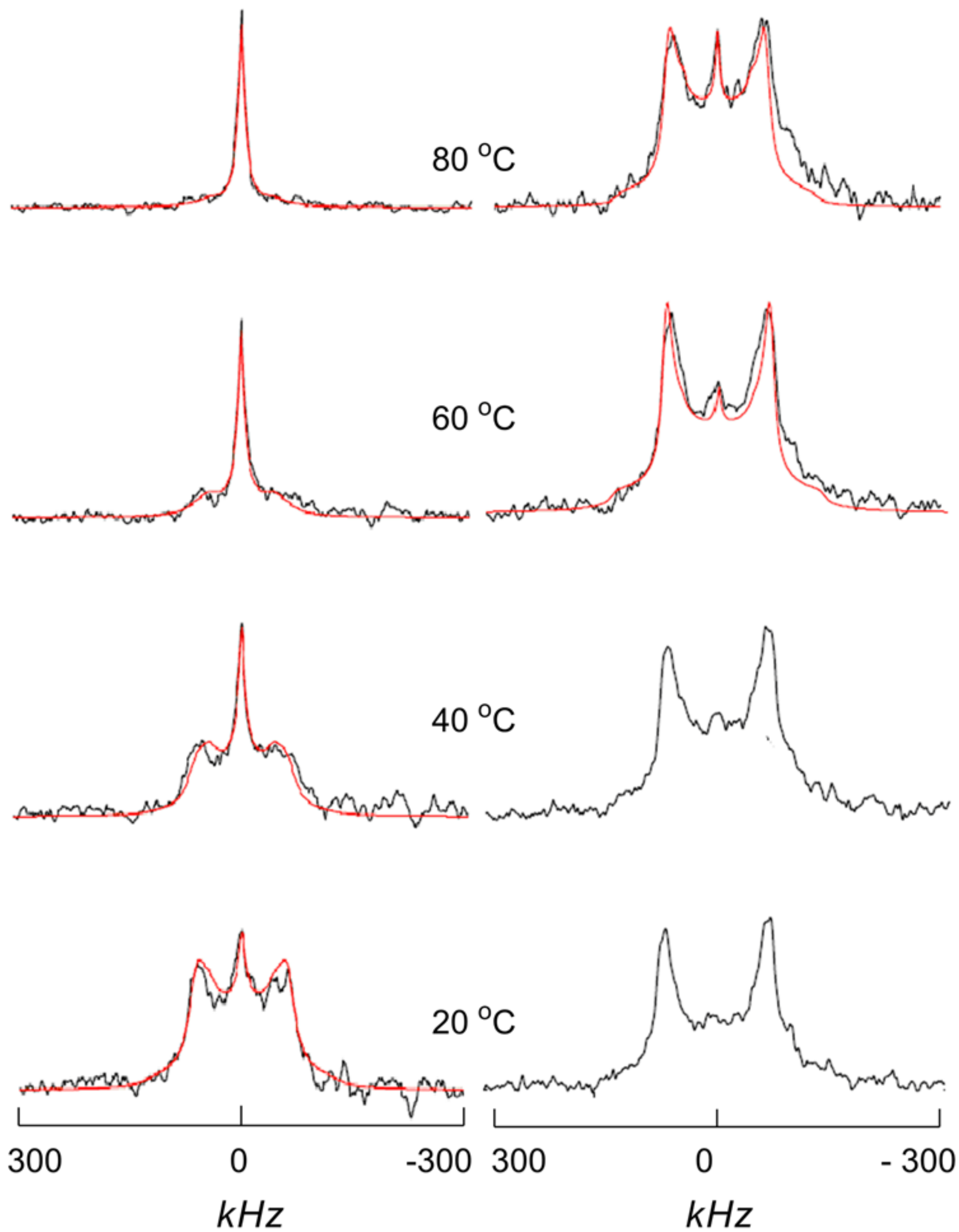

Figure 6. ^{2}H solid-state NMR spectra of **1**⊃Im-d_4 (left) and **2**⊃Im-d_4 (right). The simulation results are shown in red lines.

References:

[1] Kreuer, K. D., Paddison, S. J., Spohr, E. and Schuster, M., Transport in Proton Conductors for Fuel-Cell Applications: Simulations, Elementary Reactions, and Phenomenology. *Chem. Rev.* **104** (10), 4637 (2004).

[2] Martin F.H. Schuster and Meyer, W. H., Anhydrous Proton-Conducting Polymers. *Annu. Rev. Mater. Res.* **33**, 233 (2003).

[3] Jannasch, P., Recent developments in high-temperature proton conducting polymer electrolyte membranes. *Curr. Opin. Colloid Interface Sci.* **8** (1), 96 (2003).

[4] Li, S.et al., Synthesis and properties of imidazole-grafted hybrid inorganic-organic polymer membranes. *Electrochim. Acta* **51** (7), 1351 (2006).

[5] West, A. R., *Basic Solid State Chemistry*. (Wiley, 1999).

[6] Kawada, A., McGhie, A. R. and Labes, M. M., Protonic Conductivity in Imidazole Single Crystal. *J. Chem. Phys.* **52** (6), 3121 (1970).

[7] Noro, S., Kitagawa, S., Kondo, M. and Seki, K., A New, Methane Adsorbent, Porous Coordination Polymer. *Angew. Chem. Int. Ed.* **39** (12), 2081 (2000).

[8] Rowsell, J. L. and Yaghi, O. M., Strategies for hydrogen storage in metal-organic frameworks. *Angew. Chem. Int. Ed.* **44** (30), 4670 (2005).

[9] Ferey, G.et al., Hydrogen adsorption in the nanoporous metal-benzenedicarboxylate M(OH)(O2C-C6H4-CO2)(M = Al3+, Cr3+), MIL-53. *Chem. Commun.* (24), 2976 (2003).

[10] Rosi, N. L.et al., Hydrogen Storage in Microporous Metal-Organic Frameworks. *Science* **300** (5622), 1127 (2003).

[11] Li, H., Eddaoudi, M., O'Keeffe, M. and Yaghi, O. M., Design and synthesis of an exceptionally stable and highly porous metal-organic framework. *Nature* **402** (6759), 276 (1999).

[12] Cychosz, K. A., Wong-Foy, A. G. and Matzger, A. J., Liquid Phase Adsorption by Microporous Coordination Polymers: Removal of Organosulfur Compounds. *J. Am. Chem. Soc.* **130** (22), 6938 (2008).

[13] Finsy, V.et al., Pore-Filling-Dependent Selectivity Effects in the Vapor-Phase Separation of Xylene Isomers on the Metal-Organic Framework MIL-47. *J. Am. Chem. Soc.* **130** (22), 7110 (2008).

[14] Bradshaw, D.et al., Permanent Microporosity and Enantioselective Sorption in a Chiral Open Framework. *J. Am. Chem. Soc.* **126** (19), 6106 (2004).

[15] Dybtsev, D. N.et al., Microporous Manganese Formate: A Simple Metal-Organic Porous Material with High Framework Stability and Highly Selective Gas Sorption Properties. *J. Am. Chem. Soc.* **126** (1), 32 (2004).

[16] Min, K. S. and Suh, M. P., Self-Assembly and Selective Guest Binding of Three-Dimensional Open-Framework Solids from a Macrocyclic Complex as a Trifunctional Metal Building Block. *Chem. Eur. J.* **7** (1), 303 (2001).

[17] Wang, B.et al., Colossal cages in zeolitic imidazolate frameworks as selective carbon dioxide reservoirs. *Nature* **453** (7192), 207 (2008).

[18] Hasegawa, S.et al., Three-Dimensional Porous Coordination Polymer Functionalized with Amide Groups Based on Tridentate Ligand: Selective Sorption and Catalysis. *J. Am. Chem. Soc.* **129** (9), 2607 (2007).

[19] Horike, S., Dinca, M., Tamaki, K. and Long, J. R., Size-Selective Lewis Acid Catalysis in a Microporous Metal-Organic Framework with Exposed Mn2+ Coordination Sites. *J. Am. Chem. Soc.* **130** (18), 5854 (2008).

[20] Cho, S.-H.et al., A metal-organic framework material that functions as an enantioselective catalyst for olefin epoxidation. *Chem. Commun.* (24), 2563 (2006).

[21] Horcajada, P.et al., Synthesis and catalytic properties of MIL-100(Fe), an iron(III) carboxylate with large pores. *Chem. Commun.* (27), 2820 (2007).

[22] Schroder, F.et al., Ruthenium Nanoparticles inside Porous [Zn4O(bdc)3] by Hydrogenolysis of Adsorbed [Ru(cod)(cot)]: A Solid-State Reference System for Surfactant-Stabilized Ruthenium Colloids. *J. Am. Chem. Soc.* **130** (19), 6119 (2008).

[23] Ingleson, M. J.et al., Generation of a solid Bronsted acid site in a chiral framework. *Chem. Commun.* (11), 1287 (2008).

[24] Fujita, M., Kwon, Y. J., Washizu, S. and Ogura, K., Preparation, Clathration Ability, and Catalysis of a Two-Dimensional Square Network Material Composed of Cadmium(II) and 4,4'-Bipyridine. *J. Am. Chem. Soc.* **116** (3), 1151 (1994).

[25] Seo, J. S.et al., A homochiral metal-organic porous material for enantioselective separation and catalysis. *Nature* **404** (6781), 982 (2000).

[26] Evans, O. R., Ngo, H. L. and Lin, W., Chiral Porous Solids Based on Lamellar Lanthanide Phosphonates. *J. Am. Chem. Soc.* **123** (42), 10395 (2001).

[27] Ferey, G.et al., Mixed-Valence Li/Fe-Based Metal-Organic Frameworks with Both Reversible Redox and Sorption Properties. *Angew. Chem. Int. Ed.* **46** (18), 3259 (2007).

[28] Kitagawa, H.et al., Highly proton-conductive copper coordination polymer, H2dtoaCu (H2dtoa=dithiooxamide anion) *Inorg. Chem. Commun.* **6** (4), 346 (2003).

[29] Yamada, T., Sadakiyo, M. and Kitagawa, H., High Proton Conductivity of One-Dimensional Ferrous Oxalate Dihydrate. *J. Am. Chem. Soc.* **131** (9), 3144 (2009).

[30] Uemura, T.et al., Radical polymerisation of styrene in porous coordination polymers. *Chem. Commun.* (48), 5968 (2005).

[31] Uemura, T.et al., Conformation and Molecular Dynamics of Single Polystyrene Chain Confined in Coordination Nanospace. *J. Am. Chem. Soc.* **130** (21), 6781 (2008).

[32] Mulfort, K. L. and Hupp, J. T., Chemical Reduction of Metal-Organic Framework Materials as a Method to Enhance Gas Uptake and Binding. *J. Am. Chem. Soc.* **129** (31), 9604 (2007).

[33] Muller, M.et al., Loading of MOF-5 with Cu and ZnO nanoparticles by gas-phase infiltration with organometallic precursors: Properties of Cu/ZnO@MOF-5 as catalyst for methanol synthesis. *Chem. Mater.* **20** (14), 4576 (2008).

[34] Turner, S.et al., Direct Imaging of Loaded Metal-Organic Framework Materials (Metal@MOF-5). *Chem. Mater*. **20** (17), 5622 (2008).

[35] Horcajada, P.et al., Flexible Porous Metal-Organic Frameworks for a Controlled Drug Delivery. *J. Am. Chem. Soc.* **130** (21), 6774 (2008).

[36] Horcajada, P.et al., Metal-Organic Frameworks as Efficient Materials for Drug Delivery. *Angew. Chem. Int. Ed.* **45** (36), 5974 (2006).

[37] Tanaka, D.et al., Anthracene array-type porous coordination polymer with host-guest charge transfer interactions in excited states. *Chem. Commun.* (30), 3142 (2007).

[38] Comotti, A.et al., Nanochannels of Two Distinct Cross-Sections in a Porous Al-Based Coordination Polymer. *J. Am. Chem. Soc.* (2008).

[39] Loiseau, T.et al., A Rationale for the Large Breathing of the Porous Aluminum Terephthalate (MIL-53) Upon Hydration. *Chem. Eur. J.* **10** (6), 1373 (2004).

[40] Serre, C.et al., An Explanation for the Very Large Breathing Effect of a Metal-Organic Framework during CO2 Adsorption. *Adv. Mater.* **19** (17), 2246 (2007).

[41] Spek, A. L., Foundations of Crystallography. *Acta Crystallogr., Sect. A* **A46**, c34 (1990).

[42] Craven, B. M., McMullan, R. K., Bell, J. D. and Freeman, H. C., The crystal structure of imidazole by neutron diffraction at 20 oCand -150 oC. *Acta Crystallogr., Sect. B* **33** (8), 2585 (1977).

[43] Horike, S.et al., Motion of methanol adsorbed in porous coordination polymer with paramagnetic metal ions. *Chem. Commun.* (19), 2152 (2004).

[44] Ueda, T.et al., Phase transition and molecular motion of cyclohexane confined in metal-organic framework, IRMOF-1, as studied by 2H NMR. *Chem. Phys. Lett.* **443** (4-6), 293 (2007).

[45] Horike, S.et al., Dynamic Motion of Building Blocks in Porous Coordination Polymers13. *Angew. Chem. Int. Ed.* **45** (43), 7226 (2006).

[46] Schmidt-Rohr, K. and Spiess, H. W., *Multidimensional Solid-State NMR and Polymers*. (Academic Press, London, 1994).

[47] Abragam, A., *Principles of Nuclear Magnetism* (Oxford University Press, Oxford, 1961).

[48] Bozkurt, A. and Meyer, W. H., Proton conducting blends of poly(4-vinylimidazole) with phosphoricacid. *Solid State Ionics* **138**, 259 (2001).